MICROPLANE–TYPE CONSTITUTIVE MODELS FOR DISTRIBUTED DAMAGE AND LOCALIZED CRACKING IN CONCRETE STRUCTURES

Ignacio Carol[1], Zdeněk P. Bažant[2] and Pere C. Prat[1]
[1]ETSECCPB — Technical University of Catalonia, 08034 Barcelona, Spain
[2]Dept. of Civil Engineering, Northwestern University, Evanston, IL 60208, USA

ABSTRACT — Two constitutive formulations adequate for representing distributed damage and localized cracking of concrete are described in this paper. They are derived using the same basic idea as the microplane model, i.e. the intrinsic material behavior can be specified on a plane of generic orientation, and the macroscopic relationships derived by accumulation of the contribution from all possible directions in space. In the first formulation, based on continuum damage mechanics, a new expression of a three-dimensional damage tensor, as an integral of the damage for each microplane, is obtained. The second formulation, assuming a statically constrained microstructure, is intended to represent macroscopic cracks within the framework of smeared finite elements analysis and fracture mechanics. In that sense, two of the model parameters are the fracture energies per unit volume under modes I and II, which is convenient for adjusting their values according to the element size so as to achieve the prescribed fracture energy per unit area.

INTRODUCTION

The two formulations described in this paper are based on the idea that the intrinsic material behavior can be defined as a relationship between stresses and strains on a plane of generic orientation, and the macroscopic behavior can be derived (by application of some variational principle) as an integral or summation over all the possible orientations in space. This is in fact an old idea: Taylor in 1938 [1] and Batdorf and Budianski in 1949 [2] used it in the *"slip theory of plasticity"* for metals, and later Zienkiewicz and Pande [3], and Pande and Sharma [4], in their *"multilaminate model"* for fractured rocks and soils.

KINEMATICALLY CONSTRAINED MICROPLANE MODEL AND DAMAGE TENSOR

The first application of this idea to concrete is due to Bažant and Oh [5] under the name of *microplane model*. The present structure of the model was proposed in [6] and an optimized version in [7]. A microplane is any plane cutting the material, defined by its unit normal vector of components n_i. Normal and shear stresses σ_N, σ_{T_r} and strains ϵ_N, ϵ_{T_r} are considered on each microplane. The normal components are further split into volumetric and deviatoric parts ($\sigma_N=\sigma_V+\sigma_D$, $\epsilon_N=\epsilon_V+\epsilon_D$). The strains on the microplane ϵ_V, ϵ_D, ϵ_{T_r} are assumed equal to the projection of the strain tensor ϵ_{ij} (kinematic constraint). The stress–strain behavior of the material is specified by explicit scalar stress-strain relations $\sigma_V = \mathcal{F}_V(\epsilon_V)$, $\sigma_D = \mathcal{F}_D(\epsilon_D)$ and $\sigma_T = \mathcal{F}_T(\epsilon_T)$. The application of the principle of virtual

work leads to the expression of the macroscopic stress tensor as an integral of the stress on all the possible microplanes around a point:

$$\sigma_{ij} = \sigma_V \delta_{ij} + \frac{3}{2\pi}\int_\Omega \sigma_D n_i n_j d\Omega + \frac{3}{2\pi}\int_\Omega \frac{\sigma_{T_r}}{2}(n_i\delta_{rj} + n_j\delta_{ri} - 2n_i n_j n_r)d\Omega \quad (1)$$

In practice, integrals in (1) are performed numerically. A fixed number of "sample" directions are considerd, which serve as integration points and where, at the same time, history variables for the microplane laws are stored during computations. In [6,7] the model has proven to fit well a large number of test data under 1, 2 and 3-D loading conditions and be easy to implement and fast to run.

The microplane model can be reformulated as a continuum damage model, as described in [8]. The basic equation for a one-dimensional continuum damage model using the concepts of effective stress and strain equivalence is σ=$\alpha\tau$ where σ=macroscopic stress, τ=effective stress and α=damage variable of a geometric nature varying from 1 to 0. The corresponding expression in 3-D is $\sigma_{ij} = \alpha_{ijkm}\tau_{km}$, where damage is a fourth-order tensor (repetition of indices implies summation). The new microplane damage tensor is obtained by introducing, at the microplane level, three effective stresses τ_V, τ_D, τ_{T_r} and the corresponding damage variables α_V, α_D, α_T ($\sigma_V = \alpha_V\tau_V$, etc.). The corresponding laws for damage evolution are established in the form: $\alpha_V = \mathcal{G}_V(\epsilon_V)$, $\alpha_D = \mathcal{G}_D(\epsilon_D)$ and $\alpha_T = \mathcal{G}_T(\epsilon_T)$. The final expression gives the damage tensor as an integral of the damage in the microplanes of all possible orientations, in a purely geometric definition ("rheology" is introduced *via* the model for effective stresses τ_{km} exclusively):

$$\begin{aligned}\alpha_{ijpq} = {} & \frac{\alpha_V}{3}\delta_{ij}\delta_{pq} + \frac{3}{2\pi}\int_\Omega \alpha_D n_i n_j\Big(n_p n_q - \frac{\delta_{pq}}{3}\Big)d\Omega + \\ & + \frac{3}{2\pi}\int_\Omega \frac{\alpha_T}{4}(n_i n_p\delta_{jq} + n_i n_q\delta_{jp} + n_j n_p\delta_{iq} + n_j n_q\delta_{ip} - 4n_i n_j n_p n_q)d\Omega\end{aligned} \quad (2)$$

Two examples of application of the microplane damage tensor are presented. In the first example, described in more detail in [8], the damage model has been used in conjunction with linear elasticity for the effective stresses. The example corresponds to a uniaxial test reported by van Mier in 1984 [9], in which both longitudinal stress and transverse strain were recorded. The results are represented in Fig. 1 by solid lines. The dots are the experimental data and the dashed lines are the results obtained with the previous version of the microplane model [7]. In the second example, the microplane damage tensor has been used in conjunction with aging viscoelasticity in the form of a Maxwell chain. The parameters of the chain have been determined according to the recomendations given in [10] to approach the values of the creep function for a concrete with compressive strength f'_c=36.8 MPa, fictitious depth of the specimen e=30 cm, and relative humidity h=90%. The chain ensures that for no damage ($\alpha_{ijkm} = \delta_{ik}\delta_{jm}$, $\sigma_{ij} = \tau_{ij}$) the aging viscoelastic behavior is approached satisfactorily by the overall model. The parameters of the damage model have also been assumed to vary with time so that the peak values of the instantaneous uniaxial σ–ϵ diagram at various ages coincide with the age dependence of f'_c. Various creep tests (consisting of a uniaxial step load applied at 28 days) with increasing values of the load value, have been run with the 3-D model. The stresses and strains along the axis of loading are represented in Fig. 2 showing a strain–time diagram and a stress–strain diagram with creep isochrones. Linear creep is obtained for low stresses (under about $0.4f'_c$), and nonlinear creep and failure under sustained load is obtained under high stresses. All these features agree with the well known behavior of concrete.

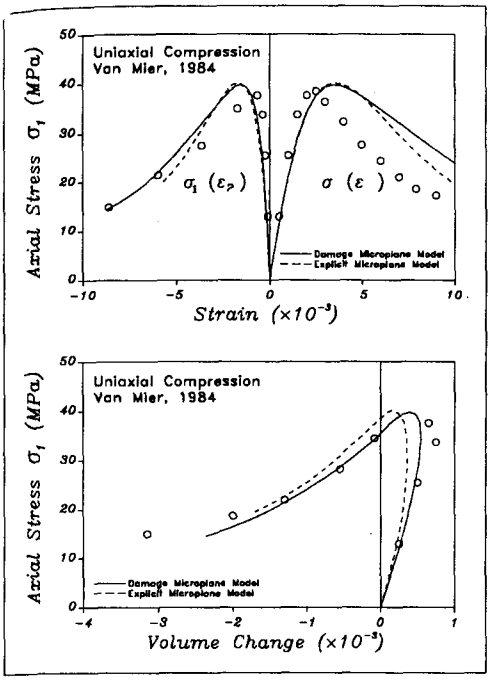

Fig. 1 — Results of example 1

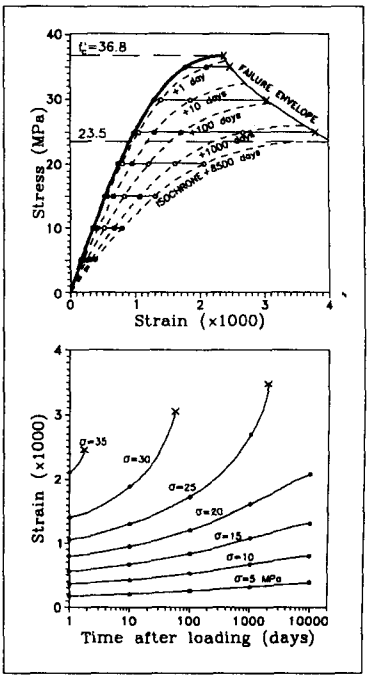

Fig. 2 — Results of example 2

MULTICRACK MODEL WITH STATIC CONSTRAINT

The multicrack model has been developed so far for 2-D analysis and is presented in more detail in [11-13]. As in other previous models for cracking, the stresses on a plane of potential cracking $\underset{\sim}{s} = [\sigma, \tau]$ are assumed equal to the projection of the stress tensor on that plane $\underset{\sim}{s}_i = \underset{\sim}{N}_i^t \underset{\sim}{\sigma}$ (static constraint), and the total macroscopic strain tensor is decomposed into the contributions of the continuum and crack components $\underset{\sim}{\varepsilon} = \underset{\sim}{\varepsilon}^{co} + \sum_{i=1}^{N_c} \underset{\sim}{\varepsilon}_i^{cr}$ with $\underset{\sim}{\varepsilon}_i^{cr} = \underset{\sim}{N}_i \underset{\sim}{e}_i^{cr}$. In these expressions

$$\underset{\sim}{N}_i^t = \begin{bmatrix} \cos^2\theta & \sin^2\theta & 2\sin\theta\cos\theta \\ -\cos\theta\sin\theta & \cos\theta\sin\theta & \cos^2\theta - \sin^2\theta \end{bmatrix} \tag{3}$$

where θ is the angle between the normal to the plane of the ith crack and the x-axis; N_c the number of existing cracks, and $\underset{\sim}{e}_i^{cr} = [\epsilon^{cr}, \gamma^{cr}]^t$ = vector of crack strain in local coordinates.

The laws of formation and evolution of a crack on a generic plane are established in terms of the local stresses (σ, τ) and strains $(\epsilon^{cr}, \gamma^{cr})$ by means of a formulation with the structure of a nonassociated plastic model. A hyperbolic "cracking surface" $F(\sigma, \tau) = 0$ with three parameters χ, c and $\tan\phi$ is assumed (Fig. 3a). Two basic modes of fracture are defined together with their corresponding fracture energies. For pure tension, the traditional mode I with associated g_f^I; and, as a second mode related to shear, the asymptotic mode IIa is defined under shear and very high compression, with associated g_f^{IIa} (Fig. 3b). These two modes represent the limiting cases of crack formation and the hyperbola provides smooth transition in between. As the crack starts, parameter ϕ is assumed to remain constant,

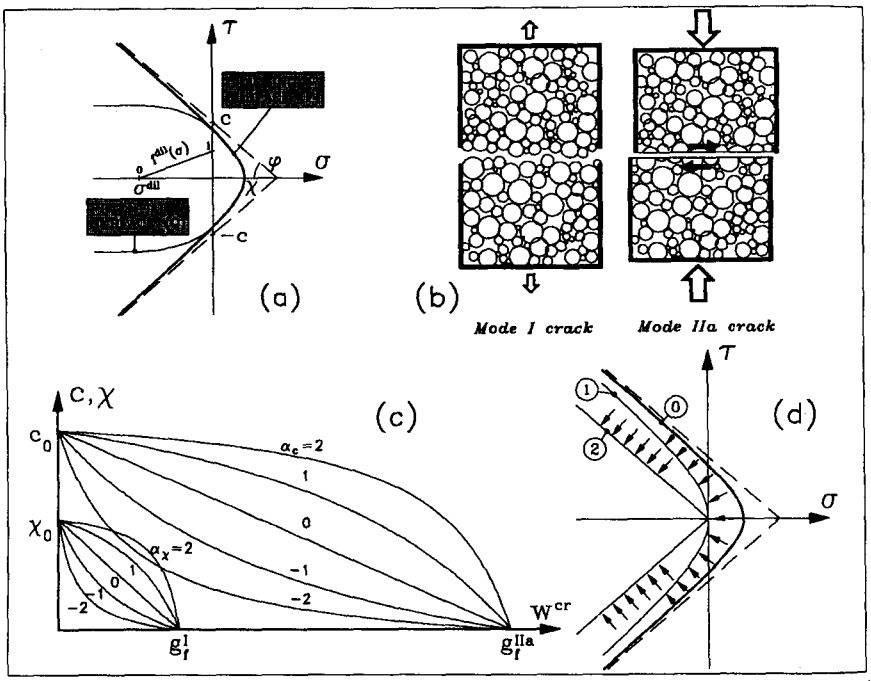

Fig. 3 — Laws for a single crack: (a) hyperbolic cracking surface F and plastic potential Q; (b) basic modes of fracture; (c) softening laws for χ and c; (d) evolution of the cracking surface

and parameters c and χ are assumed to vary with the softening variable w^{cr}, see Fig. 3c (different curves for each value of the additional parameters α_c and α_χ), where w^{cr} is the work spent on the fracture process, defined as $\mathrm{d}w^{cr} = \sigma \mathrm{d}\epsilon^{cr} + \tau \mathrm{d}\gamma^{cr}$ in tension ($\sigma > 0$), and $\mathrm{d}w^{cr} = (|\tau| - |\sigma| \tan\phi)|\mathrm{d}\gamma^{cr}|$ in compression ($\sigma < 0$), to exclude the frictional work. As the crack progresses, the cracking surface shrinks from curve 0 in Fig. 3d to curve 1 when w^{cr} reaches g_f^I, and to the pair of straight lines 2 representing pure friction when w^{cr} reaches g_f^{IIa}. The direction of the crack strain (flow rule) is given by $\mathrm{d}\underset{\sim}{\epsilon}_i^{cr} = [\partial Q/\partial \underset{\sim}{s}]_i \mathrm{d}\lambda_i$ with λ_i=plastic multiplier for the ith crack surface. The potential Q is defined so that the crack shows no dilatancy upon shear for high compressive stresses (Fig. 3a). As defined, the model has the structure of a plastic model with a number N_c of simultaneous yield surfaces. A classical derivation leads to the tangent stiffness matrix, which in this case involves the stiffness matrix of the undamaged material between the cracks:

$$\mathrm{d}\underset{\sim}{\sigma} = \underset{\sim}{D}^{crco} \mathrm{d}\underset{\sim}{\epsilon}; \quad \underset{\sim}{D}^{crco} = \underset{\sim}{D}^{co}\left(\underset{\sim}{I} - \sum_{i=1}^{N_c} \underset{\sim}{N}_i \left[\frac{\partial Q}{\partial \underset{\sim}{s}}\right]_i \left[\frac{\partial \lambda_i}{\partial \underset{\sim}{\epsilon}}\right]^t\right) \tag{4}$$

The proposed cracking model has been implemented with linear elasticity for the intact material between the cracks. Twelve fixed directions equally spaced over the upper hemicircle, are checked at each stage of the computation for new cracks forming, and old ones progressing or stopping. The first example of application at constitutive level is the direct tension test. Only one crack perpendicular to the direction of tension develops. The results are represented in Fig. 4a for different values of the parameter g_f^I. Note that the

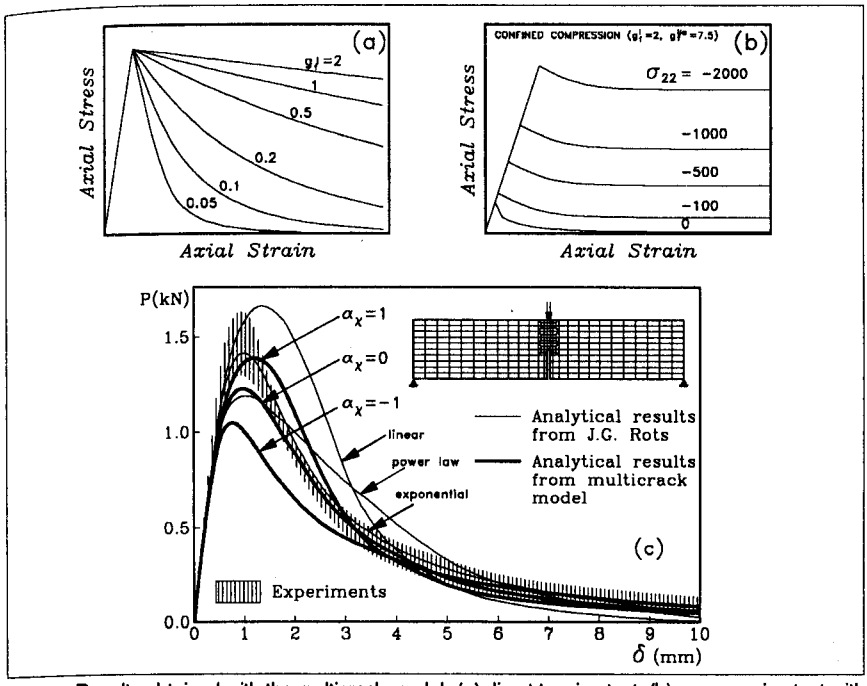

Fig. 4 — Results obtained with the multicrack model: (a) direct tension test; (b) compression test with lateral confinement; (c) finite element analysis of a three-point bending test [14]

resulting area surface under each one of the curves equals automatically the corresponding value of that parameter. The second example is a compression test with lateral confinement pressure. Two inclined cracks develop symmetrically with the inclination of about 30° on each side of the loading axis. The results for different values of the lateral pressure are represented in Fig. 4b. After the peak, the stress approaches asymptotically a final value that can be obtained from equilibrium considerations. The corner-shaped peak in the curves is due to the use of the elastic model for the continuum between the cracks. Finally, the model has been implemented in a finite element code and an example of a three-point bending beam has been analyzed. The fracture parameter g_f^I has been calculated from the experimental G_f and element size. The results obtained are shown in Fig. 4c together with experimental data [14] and numerical results from other authors [15].

CONCLUDING REMARKS

The basic idea of the microplane model, i.e. to define the basic material behavior on a plane of generic orientation and then accumulate the contributions over all possible orientations, is useful for developing new models that represent the behavior of materials undergoing damage and cracking. The new microplane damage tensor describes the geometric effects of distributed damage (microcracks). A kinematic micro–macro constraint is assumed, which corresponds to the preservation of material integrity. With the new damage tensor, the model can be combined with any existing model for the undamaged material in order to represent phenomena such as creep–damage interaction, etc. The multicrack model is intended to represent the effects of macrocracks in the context of a smeared–cracking finite element analysis of localized fracture. It is based on the static constraint, and only involves

the additional strain caused by cracks. It can be combined with any model representing the undamaged material between cracks.

The microplane model with kinematic constraint can also represent localized fracture (a crack). For the case of a pure tensile fracture (no shear crack), fracture always occurs on various microplanes within a certain range of inclinations. This might be seen unrealistic if the finite elements are large although microscopically inclined microcracks always occur. As described, the new model with static constraint cannot model complex triaxial behavior for fracture under compressive stresses, but might model a localized crack band or crack more efficiently when the narrow crack band or crack is parallel to the mesh lines and fracture can occur on microplanes of only one direction. The fracture model on these microplanes must represent frictional interlock of crack forces and dilatancy and can be specified independently of the microplane laws with kinematic constraint, which gives additional flexibility. With the kinematic constraint, the crack friction and dilatancy need not be represented by the microplane law because they are taken into account by the resistance and cracking of inclined microplanes [16], but then the shear resistance cannot be controlled independently of the opening fracture of the microplanes.

In contrast to the previous attempts at modelling of strain softening by microplanes with static constraint, this constraint is used here only for obtaining the cracking strain, while before [5] it was used for obtaining the total strains. This is the reason why previously the model turned out unstable in post-peak behavior, while the present model is stable. The kinematic constraint is not possible without calculating the total strain on the microplane level, including the elastic strain.

Acknowledgment. This paper was written during a sabatical leave of the first author at Northwestern University, funded by CIRIT (Generalitat de Catalunya, Barcelona, Spain). Financial support from research grant PB90-0598 funded by CICYT (Madrid, Spain), and from AFOSR grant 91-0141 to Northwestern University, is gratefully acknowledged.

REFERENCES

[1] G.I. Taylor (1938). *J Inst Metals* **62**, 307–324.
[2] S.B. Batdorf, B. Budianski (1949). *National Advisory Committee for Aeronautics (N.A.C.A)*, Technical Note No.1871, Washington DC.
[3] O.C. Zienkiewicz, G.N. Pande (1977). *Int J Numer Anal Meth Geomech* **1**, 219–247.
[4] G.N. Pande, K.G. Sharma (1983). *Int J Numer Anal Meth Geomech*, **7**, 397–418.
[5] Z.P. Bažant, B.H. Oh (1983), in *Symp. on The Interaction of Non-Nuclear Munitions with Structures*, US Air Force Academy, Colorado, 49–55.
[6] Z.P. Bažant, P.C. Prat (1988). *J. of Eng. Mech* ASCE, **114**(10), 1672–1702.
[7] I. Carol, Z.P. Bažant, P.C. Prat (1992). *Int. J. Sol. Struct.*, in press.
[8] I. Carol, Z.P. Bažant, P.C. Prat (1991). *J. Eng. Mech.* ASCE, **117**(10), 2429–2448.
[9] J.G.M. van Mier (1984). Ph. D. dissertation, Univ. of Eindhoven, The Netherlands.
[10] Z.P. Bažant (1989). *Mathematical Modelling of Creep and Shrinkage of Concrete*. John Wiley.
[11] I. Carol, P.C. Prat (1990), in *Computer-aided analysis and design of concrete structures*, N. Bićanić and H. Mang (eds.), Pineridge Press (UK), vol.2, 919–930.
[12] I. Carol, P.C. Prat (1991), in *Fracture processes in brittle disordered materials*, J.G.M. van Mier et al. (eds.), Chapman & Hall.
[13] P.C. Prat, I. Carol, R. Gettu (1991), in *Mixed-Mode Fracture and Fatigue*, H.P. Rossmanith (ed.), Wien.
[14] H.A. Kormeling, H.W. Reinhardt (1983). Report 5–83–18, Stevin Lab., TU Delft, The Netherlands.
[15] J.G. Rots (1988). Ph.D. thesis at TU Delft, The Netherlands.
[16] Z.P. Bažant, P. Gambarova (1984). *J Struc Eng* ASCE, **110**(9), 2015–2035.